



# Electronically synthesized Nyquist pulses for photonic sampling of microwave signals

VALERIA VERCESI,<sup>1,\*</sup> DANIEL ONORI,<sup>2</sup> JOHN DAVIES,<sup>3</sup> ALWYN SEEDS,<sup>1</sup> AND CHIN-PANG LIU<sup>1</sup>

<sup>1</sup>Department of Electronic & Electrical Engineering, University College London, Torrington Place, London WC1E 7JE, UK

<sup>2</sup>TeCip Institute, Scuola Superiore Sant'Anna Via Giuseppe Moruzzi, 1, 56127 Pisa, Italy

<sup>3</sup>THALES UK, 350 Longwater Avenue, Green Park, Reading, RG2 6GF, UK

\*v.vercesi@ucl.ac.uk

**Abstract:** We report electronic generation of optical Nyquist pulses using an arbitrary waveform generator (AWG) followed by a Mach Zehnder modulator (MZM), providing a simple, highly stable and flexible technique to perform photonic sampling. Here, we demonstrate the generation of 10 GHz periodic optical Nyquist pulses by synthesizing both all-positive and alternate positive-negative electrical pulse trains using a 25 GHz bandwidth AWG. Biasing the MZM at null ensures the meeting of the Nyquist ISI-free criterion in the optical domain and allows for pulse compression. Moreover, we report the first photonic sampling and demodulation of 1 Gbaud 16- and 32-QAM signals up to 22.5 GHz using 10 GHz optical Nyquist sampling pulse trains.

Published by The Optical Society under the terms of the [Creative Commons Attribution 4.0 License](https://creativecommons.org/licenses/by/4.0/). Further distribution of this work must maintain attribution to the author(s) and the published article's title, journal citation, and DOI.

**OCIS codes:** (060.5625) Radio frequency photonics; (070.1170) Analog optical signal processing; (320.5550) Pulses; (350.4010) Microwaves.

## References and links

1. H. Taylor, "An optical analog-to-digital converter - Design and analysis," *IEEE J. Quantum Electron.* **15**(4), 210–216 (1979).
2. P. Ghelfi, F. Laghezza, F. Scotti, G. Serafino, A. Capria, S. Pinna, D. Onori, C. Porzi, M. Scaffardi, A. Malacarne, V. Vercesi, E. Lazzeri, F. Berizzi, and A. Bogoni, "A fully photonics-based coherent radar system," *Nature* **507**(7492), 341–345 (2014).
3. G. C. Valley, "Photonic analog-to-digital converters," *Opt. Express* **15**(5), 1955–1982 (2007).
4. F. Su, G. Wu, L. Ye, R. Liu, X. Xue, and J. Chen, "Effects of the photonic sampling pulse width and the photodetection bandwidth on the channel response of photonic ADCs," *Opt. Express* **24**(2), 924–934 (2016).
5. T. R. Clark, J. U. Kang, and R. D. Esman, "Performance of a time- and wavelength-interleaved photonic sampler for analog-digital conversion," *IEEE Photonics Technol. Lett.* **11**(9), 1168–1170 (1999).
6. J. U. Kang and R. D. Esman, "Demonstration of time interweaved photonic four-channel WDM sampler for hybrid analogue-digital converter," *Electron. Lett.* **35**(1), 60–61 (1999).
7. M. Y. Frankel, J. U. Kang, and R. D. Esman, "High-performance photonic analogue-digital converter," *Electron. Lett.* **33**(25), 2096–2097 (1997).
8. J. Kim, M. J. Park, M. H. Perrott, and F. X. Kärtner, "Photonic subsampling analog-to-digital conversion of microwave signals at 40-GHz with higher than 7-ENOB resolution," *Opt. Express* **16**(21), 16509–16515 (2008).
9. A. Khilo, S. J. Spector, M. E. Grein, A. H. Nejadmalayeri, C. W. Holzwarth, M. Y. Sander, M. S. Dahlem, M. Y. Peng, M. W. Geis, N. A. DiLello, J. U. Yoon, A. Motamedi, J. S. Orcutt, J. P. Wang, C. M. Sorace-Agaskar, M. A. Popović, J. Sun, G.-R. Zhou, H. Byun, J. Chen, J. L. Hoyt, H. I. Smith, R. J. Ram, M. Perrott, T. M. Lyszczarz, E. P. Ippen, and F. X. Kärtner, "Photonic ADC: overcoming the bottleneck of electronic jitter," *Opt. Express* **20**(4), 4454–4469 (2012).
10. A. O. J. Wiberg, L. Liu, Z. Tong, E. Myslivets, V. Ataie, B. P.-P. Kuo, N. Alic, and S. Radic, "Photonic preprocessor for analog-to-digital-converter using a cavity-less pulse source," *Opt. Express* **20**(26), B419–B427 (2012).
11. I. Morohashi, T. Sakamoto, H. Sotobayashi, T. Kawanishi, I. Hosako, and M. Tsuchiya, "Widely repetition-tunable 200 fs pulse source using a Mach-Zehnder-modulator-based flat comb generator and dispersion-flattened dispersion-decreasing fiber," *Opt. Lett.* **33**(11), 1192–1194 (2008).

12. A. O. J. Wiberg, C. S. Bres, B. P. P. Kuo, J. X. Zhao, N. Alic, and S. Radic, "Pedestal-Free Pulse Source for High Data Rate Optical Time-Division Multiplexing Based on Fiber-Optical Parametric Processes," *IEEE J. Quantum Electron.* **45**(11), 1325–1330 (2009).
13. M. Nakazawa, T. Hirooka, P. Ruan, and P. Guan, "Ultra-high-speed "orthogonal" TDM transmission with an optical Nyquist pulse train," *Opt. Express* **20**(2), 1129–1140 (2012).
14. T. Hirooka, P. Ruan, P. Guan, and M. Nakazawa, "Highly dispersion-tolerant 160 Gbaud optical Nyquist pulse TDM transmission over 525 km," *Opt. Express* **20**(14), 15001–15007 (2012).
15. M. A. Soto, M. Alem, M. Amin Shoaie, A. Vedadi, C. S. Brès, L. Thévenaz, and T. Schneider, "Optical sinc-shaped Nyquist pulses of exceptional quality," *Nat. Commun.* **4**, 2898 (2013).
16. J. D. McKinney, "Technology: Photonics illuminates the future of radar," *Nature* **507**(7492), 310–311 (2014).
17. G. J. Proakis and M. Salehi, *Digital Communications*, 5<sup>th</sup> ed. (McGraw-Hill, 2008).

## 1. Introduction

Digital signal processing (DSP) is a powerful technique for storing, analyzing and manipulating digital signals. Ultimately, the quality of the signal to be processed is determined by the performance of the analog-to-digital converter (ADC) which is used to sample the original analog signal in the first place and produce a digital representation of it. Photonics has been used to increase the performance of electronic ADCs since the 1970s [1], to the extent that the first fully photonics-based radar system has already been realized [2]. Many demonstrated photonic ADC systems [3] have traditionally employed mode-locked lasers as the sampling pulse sources [4–9]. However, such pulsed optical sources require constant stability adjustments and do not allow flexible sampling frequencies.

A number of alternative optical pulse generation techniques have been proposed and demonstrated. In [10], a 2 GHz 3 ps cavity-less pulse source is reported where a CW light source was first chirped with two phase modulators, carved and gated into pulses with two other Mach Zehnder modulators (MZM), and finally compressed using 64 m of dispersion compensating fiber. In [11], 200 fs pulse trains of up to 17 GHz were generated using a MZM based optical comb generator followed by frequency compensation with a single mode fiber (SMF) and further pulse compression with a dispersion-flattened dispersion-decreasing fiber. A 40 GHz 1.2 ps pulse source has also been reported [12] where the optical pulses were initially produced by a MZM driven with an electrical 40 GHz sine wave, then spectrally broadened using self-phase modulation and finally compressed in a one-pump fiber-optic parametric amplifier.

Recently, all-optical generation of sinc-shaped Nyquist pulses has attracted increasing attention because of their tolerance to inter-symbol interference (ISI) and high spectral efficiency [13] which are important for optical time division multiplexing (OTDM) applications [14]. One such generation technique involves manipulating the spectral components of the Gaussian-shaped output pulses from a mode-locked laser into 40 GHz Nyquist pulses [13]. A more flexible generation technique directly synthesizes a 156 GHz wide rectangular-shaped and phase-locked optical frequency comb, required for a 26 GHz sinc-shaped pulse train, by externally modulating a CW laser source with a cascade of RF driven MZMs [15].

Direct sampling of microwave frequency signals with Nyquist pulses as the first step of analog-to-digital conversion is expected to find applications in wireless communications, antenna remoting and radar systems [16]. Although the aforementioned Nyquist pulse generation techniques are applicable to the sampling of microwave frequency signals, their implementations can be complicated as they require careful electrical/optical path matching, frequency multiplication, and/or more than one modulator. Electronic generation of optical Nyquist pulses using an arbitrary waveform generator (AWG) and a MZM, on the other hand, represents a simpler, highly stable and flexible technique, affording precise control of the repetition rate and pulse shape as well as the pulse amplitude. Repetition rates of over 10 GHz and pulse widths of the order of tens of ps are now obtainable with modern high-speed AWGs. The frequency responses of the AWG itself, microwave cables, amplifiers as well as

the MZM used, which would otherwise degrade the pulse shape, can be easily pre-compensated and corrected.

In this work, we investigate the generation of 10 GHz optical Nyquist pulses by driving a MZM with both all-positive and alternate positive-negative electrical pulse trains synthesized using a 25 GHz AWG. By biasing the MZM at  $V_{\pi}$  (null), the zero-crossing points of the input electrical Nyquist pulse trains translate into the zero-power points of the output optical Nyquist pulse trains, thus meeting the Nyquist ISI-free criterion [17]. We show that the resulting optical pulse width is reduced with respect to the electrical one from the AWG output. Finally, we report the first photonic sampling and demodulation of 1 Gbaud 16-QAM and 32-QAM signals using 10 GHz optical Nyquist pulse trains, achieving low error vector magnitude (EVM) values of less than 6% up to a carrier frequency of 22.5 GHz.

## 2. Synthesis of Nyquist pulses

We generate optical periodic Nyquist pulses with a 10 GHz repetition rate, suitable for photonic sampling operations, starting from electronically synthesized periodic Nyquist pulses. To this end, we calculate the pulse waveform files to be loaded to the AWG to generate the electrical signals for driving the MZM, which in turn produces the optical pulses for the photonic sampling process. The periodic pulse trains can be constructed using either a sequence of all-positive or alternate positive-negative pulses. The two types of Nyquist pulse trains are described and compared in this section.

A single, positive Nyquist pulse is generally described in the time-domain by Eq. (1):

$$h(t) = \frac{\sin\left(\frac{\pi t}{T_s}\right) \cos\left(\frac{\pi\beta t}{T_s}\right)}{\left(\frac{\pi t}{T_s}\right) \left(1 - \left(\frac{2\beta t}{T_s}\right)^2\right)} \quad (1)$$

where  $T_s$  is the pulse duration between zero-crossings and  $\beta$  is the roll-off factor. Theoretically, even a single Nyquist pulse should last indefinitely, starting from negative infinity in time, through time zero when the peak of the pulse occurs, to positive infinity in time. In practice, however, each of the pulses must be truncated to a finite time span for signal synthesis and generation by an AWG.

The shortest achievable pulse width is ultimately determined by the analog bandwidth or the highest frequency output of the AWG, which is 25 GHz in our experimental arrangement. With this in mind,  $T_s$  and  $\beta$  should then be chosen to avoid generating any signal components higher than 25 GHz while aiming to achieve the shortest possible pulse width. Assuming  $T_s = 25$  ps and  $\beta = 0.5$ , the single-sided bandwidth of a single Nyquist pulse is therefore  $B = (1 + \beta)/(2T_s) = 30$  GHz. The calculated continuous frequency spectrum of such a pulse is shown by the red curve in Fig. 1(a) which verifies that there is no spectral content at 30 GHz and above.

Although the red curve in Fig. 1(a) suggests that the generation of such a single Nyquist pulse would require an AWG capable of outputting up to 30 GHz, it is noted that an all-positive, periodic pulse train with the same  $T_s$  and  $\beta$  will exhibit an FFT spectrum with discrete spectral lines. The relative amplitudes of these discrete spectral lines follow that of the continuous frequency spectrum of the corresponding single pulse. Therefore, if the pulse repetition rate is set to 10 GHz, the corresponding frequency spectrum will only have discrete spectral lines at 0 Hz, 10 GHz and 20 GHz since the chosen  $T_s$  and  $\beta$  suppress all spectral contents from 30 GHz upwards as shown by the blue spectral lines in Fig. 1(a). This also

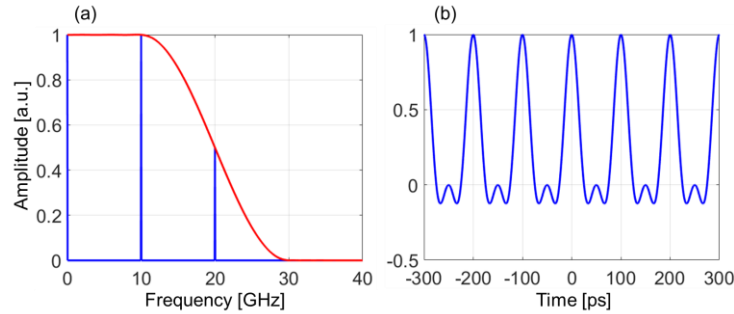


Fig. 1. Numerical simulations showing: (a) frequency spectra of one single Nyquist pulse (red) and the corresponding 10 GHz all-positive periodic pulse train (blue) with  $\beta=0.5$  and  $T_s=25$  ps ; (b) time-domain waveform of the 10 GHz all-positive Nyquist periodic pulse train.

means that although the 25 GHz AWG does not have sufficient bandwidth to generate a single Nyquist pulse with the desired  $T_s$  and  $\beta$ , it is capable of generating a periodic, all-positive Nyquist pulse train using the same  $T_s$  and  $\beta$ .

The periodic pulse train is obtained by summing a series of uniformly time-shifted individual Nyquist pulses, each truncated to the length of  $\pm S/2$  from the pulse peak according to the following equations:

$$y(t) = \sum_{n=-M/2}^{M/2} g(t-nT) \quad (2)$$

$$\text{where } g(t-nT) = \begin{cases} 0 & \text{when } |t-nT| > \frac{S}{2} \\ h(t-nT) & \text{when } |t-nT| \leq \frac{S}{2} \end{cases} \quad (3)$$

where  $T=100$  ps is the time interval of the 10 GHz pulse train,  $S=20T_s=0.5$  ns is the span of each pulse, and  $M$  is the number of time-shifted pulses used. Therefore, the total number of Nyquist pulses in the above summation is  $M+1$  which should be chosen so that the time from the first to the last pulse peak is at least twice the pulse span, i.e.  $2S$ . This is to ensure that when the middle half of the waveform array centered at  $t=0$  is selected from Eq. (2) for upload to the AWG, the end of the selected waveform array will transition smoothly to the start of the same array as the AWG plays back the uploaded waveform continuously in a loop. Furthermore, individual pulses are orthogonal to each other in the time-domain as the time interval of the periodic pulse train is a multiple of the time duration between zero-crossings, i.e.  $T=4T_s$ , and therefore individual pulse peaks only occur at the zero-crossing points of other pulses. Figure 1(b) plots a segment of the calculated 10 GHz periodic Nyquist pulse train. With  $T_s=25$  ps and  $\beta=0.5$ , the calculated full width at half maximum (FWHM) of the periodic all-positive Nyquist pulse train is 28.7 ps before any compression.

A second approach is to use alternate positive-negative Nyquist pulses, which, as will be shown shortly, can make full use of the 25 GHz AWG bandwidth leading to a shorter FWHM but will require a larger drive amplitude to achieve the same pulse peak level. The following equation is used for the alternate positive-negative pulse train generation:

$$y(t) = \sum_{n=-M/2}^{(M/2)-1} (-1)^n g(t - nT - 0.5T) \quad (4)$$

$$\text{where } g(t - nT - 0.5T) = \begin{cases} 0 & \text{when } |t - nT - 0.5T| > \frac{S}{2} \\ h(t - nT - 0.5T) & \text{when } |t - nT - 0.5T| \leq \frac{S}{2} \end{cases} \quad (5)$$

Due to its alternate nature, this positive-negative pulse train possesses different spectral features to that of the all-positive pulse train. Firstly, it does not have a DC level. Secondly, the fundamental frequency is now at 5 GHz instead of the previous 10 GHz. Thirdly, the only other higher harmonics are now at 15 GHz and 25 GHz as the current combination of  $T_s$  and  $\beta$  filters out any spectral contents from 30 GHz upwards. However, it is noted that this periodic positive-negative pulse train does not contain a spectral line at 30 GHz and the next would-be harmonic component at 35 GHz can still be filtered out even if  $\beta$  is increased to 0.75. Increasing  $\beta$  to 0.75 further decreases the corresponding FWHM, before MZM compression, from 28.7 ps using the all-positive pulses, to 27 ps using the alternate positive-negative pulses while still staying within the 25 GHz bandwidth of the AWG. The corresponding frequency spectrum and the pulse train are plotted in Fig. 2.

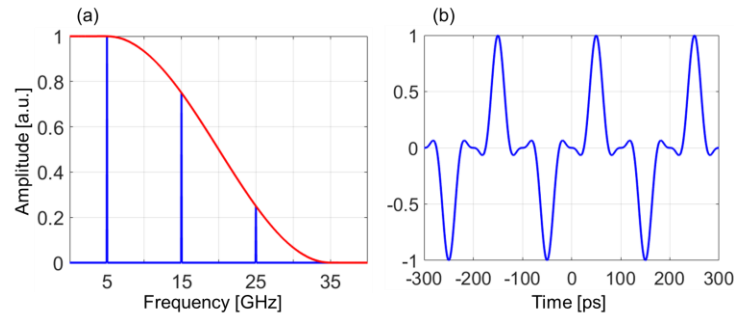


Fig. 2. Numerical simulations showing: (a) frequency spectra of one single Nyquist pulse (red) and the corresponding 10 GHz alternate positive-negative periodic pulse train (blue) with  $\beta=0.75$  and  $T_s=25$  ps; (b) time-domain waveform of the 10 GHz alternate positive-negative Nyquist periodic pulse train.

The optical Nyquist pulses can be obtained by pulse carving with an MZM driven by the AWG. To maintain orthogonality in the carved optical pulses and meet the Nyquist ISI-free criterion, the DC bias voltage for the MZM should be set so that the zero-crossing points of the AWG generated Nyquist pulse trains are at the half-voltage of the MZM,  $V_{\pi}$ , at which the output optical power should ideally be zero. The negative parts of the electrical pulse trains are “flipped” upwards about zero voltage level. The pulse carving process for both pulse trains is illustrated in Fig. 3. It is evident from Fig. 3 that to achieve the same output optical peak power, the necessary AWG peak-to-peak output voltage driving the MZM is almost twice as large for generating the alternate positive-negative pulse train as for the all-positive one. In any case, an electrical amplifier is required to increase the input voltage to the MZM.

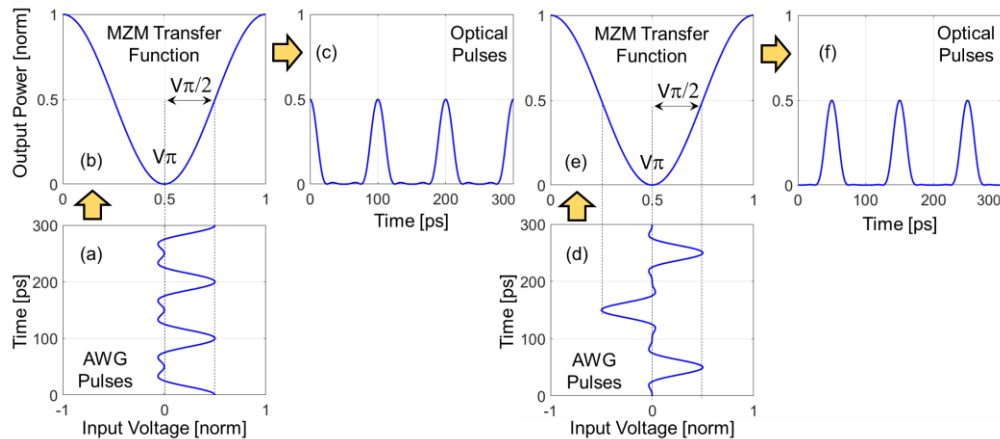


Fig. 3. Numerical simulations showing the optical Nyquist pulse generation by pulse carving with a MZM which is driven with the electrical Nyquist pulses from the AWG. (a) Electrical, all-positive Nyquist pulses with  $\beta = 0.5$  and  $T_s = 25$  ps generated by the AWG; (b) MZM transfer function and (c) 10 GHz carved optical Nyquist pulses from (a). (d) Electrical, alternate positive-negative Nyquist pulses with  $\beta = 0.75$  and  $T_s = 25$  ps generated by the AWG; (e) MZM transfer function and (f) 10 GHz carved optical Nyquist pulses from (d). The zero-crossing points of the AWG generated Nyquist pulse trains are set at the  $V_\pi$  of the MZM so that the negative parts of the electrical pulse trains are “flipped” upwards about the zero-voltage level. In the labels, “norm” stands for “normalized”.

The concave-upward transfer characteristic of the MZM around  $V_\pi$  can be exploited to achieve further reduction in the FWHM of the carved pulses and to reduce the amplitude of the small signals in-between pulses. The amount of pulse compression is a function of the peak voltage of the input electrical Nyquist pulses to the MZM as calculated and plotted in Fig. 4. It can be seen in Fig. 4 that the pulse FWHM increases with increasing pulse peak voltage. When the pulse peak voltage is the same as  $V_\pi$ , there is no pulse compression. Therefore, the pulse peak voltage is a trade-off between having a sufficient optical peak power and a short enough pulse FWHM. As an example, for the all-positive pulse train with  $T_s = 25$  ps,  $\beta = 0.5$  and the peak voltage set to  $0.5V_\pi$ , the calculated FWHM of the optical pulses is 22.5 ps. For the alternate positive-negative pulse train with  $T_s = 25$  ps,  $\beta = 0.75$  and the peak voltage also set to  $0.5V_\pi$ , the calculated FWHM of the optical pulses is 21.1 ps. Both examples demonstrate a calculated pulse width compression of about 22%.

The calculated Nyquist pulse waveform files were uploaded to the AWG for signal generation. However, due to the non-ideal or non-flat frequency responses of the components used, the pulse shape of the AWG generated pulses was initially different from the simulation results. In particular, the AWG frequency response is not flat over its full 25 GHz output bandwidth because of the zero-order hold output digital-to-analog converter (DAC) characteristics. Also, the cables, amplifier as well as the MZM exhibit frequency dependent signal attenuations and group delays.

As these frequency responses that degrade the pulse shape originate from linear effects, a digital least-mean-squares (LMS) adaptive filter has been implemented to obtain a compensation filter impulse response that can then be used to pre-compensate the pulse train waveform and correct for the pulse shape. Since the MZM pulse compression is a nonlinear process, to include the MZM frequency response in the adaptive filtering process, the

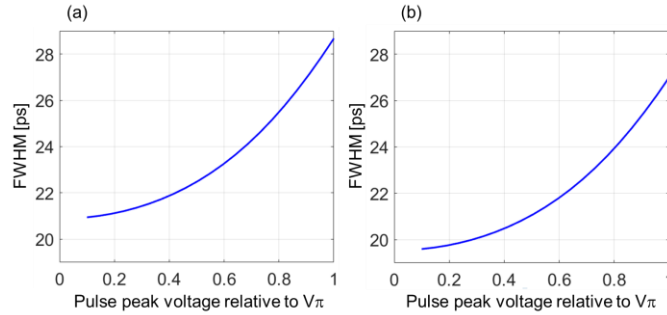


Fig. 4. Calculated FWHM of the carved optical pulses as a function of the electrical pulse peak voltage relative to  $V_\pi$  of the MZM for (a) all-positive Nyquist pulses with  $\beta = 0.5$  and  $T_s = 25$  ps, and (b) alternate positive-negative Nyquist pulses with  $\beta = 0.75$  and  $T_s = 25$  ps.

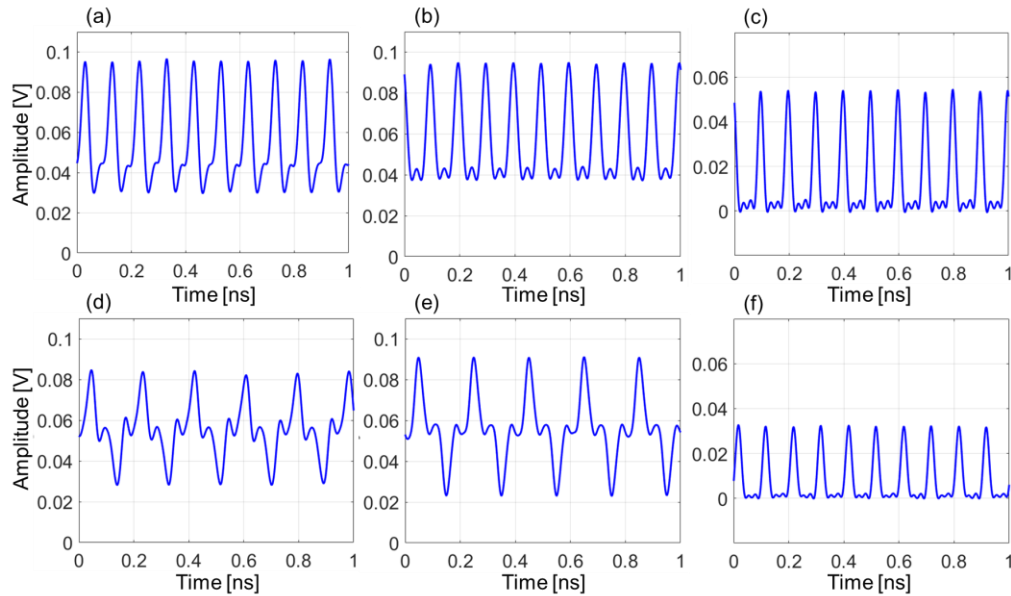


Fig. 5. Photodetected optical Nyquist pulse trains from (a) uncompensated all-positive Nyquist pulses with the MZM biased at  $3V_\pi/2$ ; (b) compensated all-positive Nyquist pulses with the MZM biased at  $3V_\pi/2$  and (c) compensated all-positive Nyquist pulses after the MZM bias voltage was changed to  $V_\pi$ . Photodetected optical Nyquist pulse trains from (d) uncompensated alternate positive-negative Nyquist pulses with the MZM biased at  $3V_\pi/2$ ; (e) compensated alternate positive-negative Nyquist pulses with the MZM biased at  $3V_\pi/2$  and (f) compensated alternate positive-negative Nyquist pulses after the MZM bias voltage was changed to  $V_\pi$ .

amplitude of the pulse train driving the MZM needed to be much reduced and the MZM was biased at  $3V_\pi/2$ . Effectively, the MZM was temporarily operated as a linear intensity modulator rather than a pulse carver/compressor during the adaptive filtering. The ideal Nyquist waveform was then compared with the photodetected pulse train using the LMS adaptive filter in LabVIEW resulting in an impulse response represented by 128 coefficients. Calculating the adaptive filter frequency response using these coefficients reveals that to compensate the all-positive Nyquist pulse train, the filter applied about 3 dB gain to the 20

GHz component relative to the 10 GHz one. To compensate the alternate positive-negative Nyquist pulse train, the filter applied about 3 dB and 10 dB gain, respectively, to the 15 GHz and 25 GHz components relative to the 5 GHz one. The filter impulse response was then convolved with the original waveform file, thus producing a new, frequency pre-compensated Nyquist pulse train waveform file for upload to the AWG. Figure 5 shows the photodetected Nyquist pulse trains before and after frequency pre-compensation when the MZM was biased at  $3V_{\pi}/2$ , and after compression with the MZM biased at  $V_{\pi}$ . In this example, both the all-positive and alternate positive-negative pulses were generated with the same peak-to-peak amplitude. Therefore, after the compression, the optical pulses obtained from the alternate positive-negative electrical Nyquist pulses in Fig. 5(f) show a smaller peak amplitude compared with those from the all-positive ones in Fig. 5(c). The generated pulses showed an optical signal-to-noise ratio higher than 30 dB.

### 3. Photonic sampling experiment with Nyquist pulses

The optical Nyquist pulses, generated using both techniques described above, were employed in a classic, photonic assisted analog-to-digital converter architecture [3] based on the use of a Mach Zehnder modulator to perform the optical sampling of an incoming signal. The implemented architecture is shown in Fig. 6.

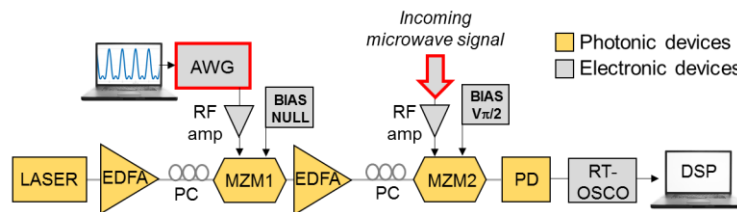


Fig. 6. Photonic assisted ADC architecture based on a cavity-less Nyquist pulse source. AWG: arbitrary waveform generator; RF amp: electrical amplifier; PC: polarization controller; MZM1,2: Mach Zehnder modulator; EDFA: Erbium doped fiber amplifier; PD: photodiode; RT-OSCO: real-time oscilloscope; DSP: digital signal processing.

The output of a CW, narrow linewidth, 1549 nm wavelength fiber laser was first optically amplified to 13 dBm before being sent to a 40 GHz Photline Lithium Niobate intensity modulator (MZM1) acting as a pulse carver. An 8-bit Keysight M8195A AWG with a 25 GHz output bandwidth and an intrinsic jitter of approximately 110 fs (rms) at 10 GHz was used to generate the pre-compensated electrical Nyquist pulses. The pulse amplitude was then amplified to  $6.3V_{pp}$  for both all-positive and alternate positive-negative pulse trains. The amplified electrical Nyquist pulses then drove MZM1, which was biased at  $V_{\pi}$  to achieve pulse compression from the nonlinear, concave-upward transfer characteristic of the modulator around the null point.

After further optical amplification, the carved 10 GHz optical Nyquist pulses with a peak pulse power of 32 mW and a FWHM of around 24 ps for both types of pulses were sent to the sampling stage where a second 40 GHz intensity modulator (MZM2), biased at its quadrature point, was driven with the incoming microwave signal to be sampled. This second modulator MZM2 was a TeraXion Indium Phosphide Mach Zehnder intensity modulator with an insertion loss of 7 dB and a low  $V_{\pi}$  of 2.5 V. Photonic sampling of the incoming microwave signal was therefore achieved by the external intensity modulation of the 10 GHz optical Nyquist pulses passing through MZM2.

To perform analog-to-digital conversion on the sampled signal, the modulated optical Nyquist pulses were first photodetected with a broadband photodiode. The received average power was 2.5 dBm. The photodetected Nyquist pulses were then captured with a 36 GHz real-time LeCroy oscilloscope acting as the analog-to-digital converter. Although the pulse

repetition rate, and hence the signal sampling frequency, was only 10 GHz, the real-time oscilloscope was configured to capture the input signal at 80 GSa/s, which is a necessary condition for using the full 36 GHz input electrical bandwidth. The oscilloscope was synchronized with the AWG so that the received Nyquist pulse peaks were captured precisely at one out of every eight sampling instances by the oscilloscope. An alternative approach would be to employ a 10 GSa/s digitizer, synchronized with the Nyquist pulse peaks, without any anti-aliasing filter at the input. The captured waveform was then repeatedly transferred from the oscilloscope to a computer for digital signal processing (DSP) in LabVIEW, including decimating or down-sampling the waveform from 80 GSa/s to 10 GSa/s, retaining only those samples holding the amplitude values of the pulse peaks.

The frequency response of the photonic sampling system was first characterized using sinusoidal signals from 1 GHz to 19.5 GHz as the input to MZM2. The amplitudes of the sampled sinusoids were obtained by performing Fast Fourier Transform (FFT) on the decimated, 10 GSa/s waveform samples. Since the sampling rate was 10 GSa/s, those input sinusoids below 5 GHz were directly sampled. Those input sinusoids above 5 GHz were bandpass sampled and their amplitudes were obtained from the region of the FFT spectrum below 5 GHz, the so-called first Nyquist zone. Figure 7 shows the measured frequency response of the sampling system relative to that at 1 GHz using all-positive Nyquist pulses. A separate measurement using CW light instead of optical pulses confirmed that the frequency response in Fig. 7 was due to those of MZM2 and the connecting microwave cables.

Finally, photonic sampling and demodulation of vector modulated microwave signals was performed. Both 16-QAM and 32-QAM signals at 1 Gbaud with carrier frequencies at 2.5 GHz, 12.5 GHz, 17.5 GHz and 22.5 GHz were generated using the AWG and input to MZM2. All the QAM signals were amplified to 10 dBm before being input to MZM2. The root raised cosine function with a roll-off factor of 0.35 was used for shaping the QAM signals, leading to a modulation bandwidth of 1.35 GHz. All the carrier frequencies were chosen so that after either direct or bandpass sampling at 10 GSa/s, the sampled QAM signals would all be centered at 2.5 GHz. Both all-positive and alternate positive-negative electrical pulses were used. Demodulation and analysis of the sampled QAM signals was performed in LabVIEW with the same root raised cosine pulse-shaping filter. Figure 8 shows the measured constellation diagrams and the corresponding error vector magnitude (EVM) values for both 16- and 32-QAM signals of different carrier frequencies. Both all-positive and alternate positive-negative pulse trains produced very similar EVM values for the same modulation format and carrier frequency, and the largest measured EVM was still less than 6% at the highest carrier frequency of 22.5 GHz. The results in Fig. 8 demonstrate the capability of the proposed photonic sampling technique in sampling and processing ultra-wideband (at least 1 GHz bandwidth) microwave signals with multilevel vector modulation formats.

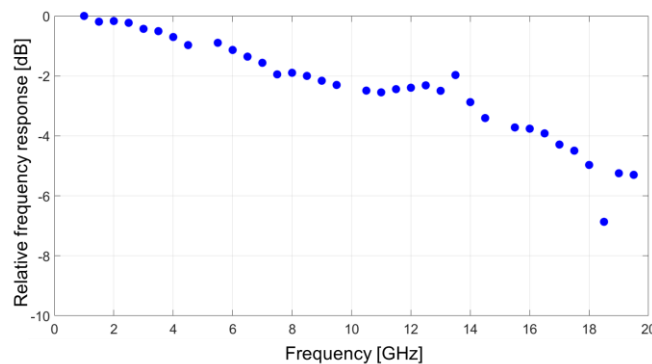


Fig. 7. Measured relative frequency response of the overall photonic sampling system using 10 GHz Nyquist sampling pulses from an electrical, all-positive pulse train.

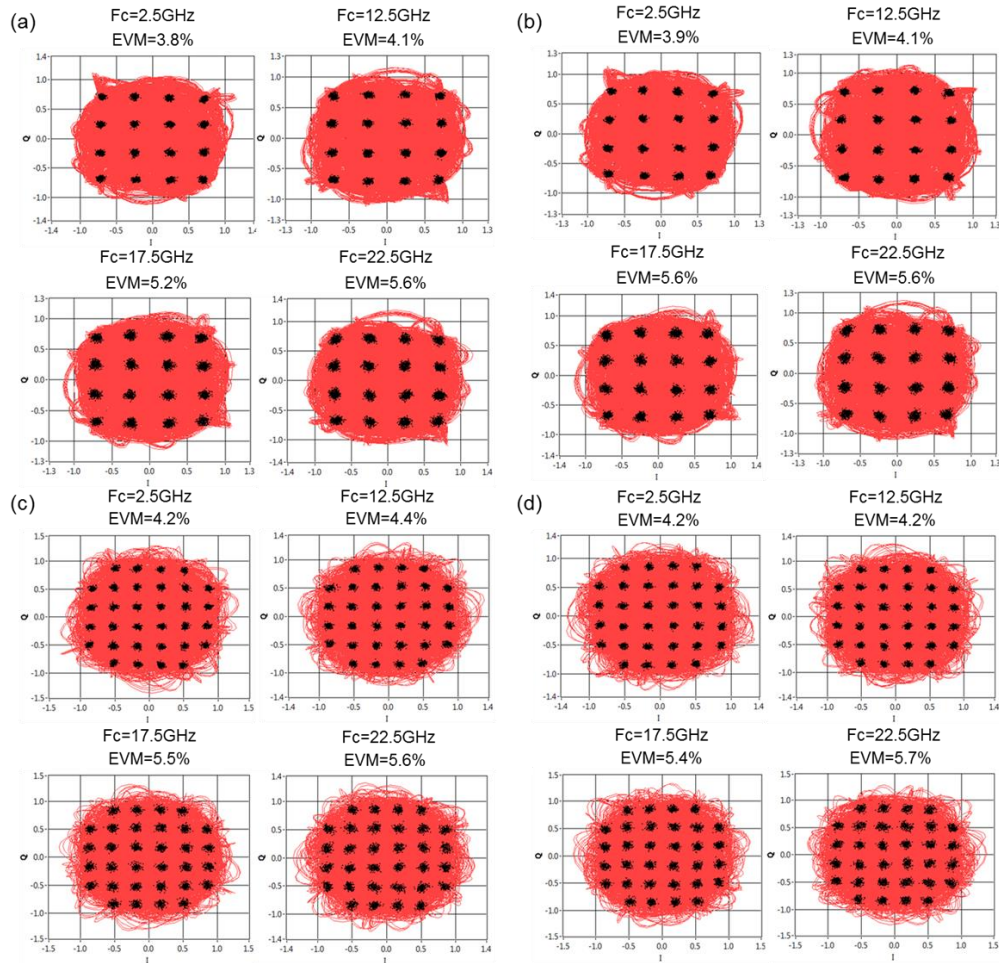


Fig. 8. Constellation diagrams and EVM values of (a) 1 Gbaud 16-QAM signals sampled with all-positive 10 GHz Nyquist pulses; (b) 1 Gbaud 16-QAM signals sampled with alternate positive-negative 10 GHz Nyquist pulses; (c) 1 Gbaud 32-QAM signals sampled with all-positive 10 GHz Nyquist pulses; (d) 1 Gbaud 32-QAM signals sampled with alternate positive-negative 10 GHz Nyquist pulses. Fc: Carrier frequency of the incoming QAM signals.

#### 4. Conclusion

Electronic generation of optical Nyquist pulses using an arbitrary waveform generator and a Mach Zehnder modulator represents a simple, highly stable and flexible technique, affording precise control of the repetition rate, the pulse shape and the pulse amplitude. In this work, we showed for the first time, to the best of our knowledge, the generation of 10 GHz optical Nyquist pulse trains using an AWG and a MZM for photonic sampling of vector modulated microwave signals. Either all-positive or alternate positive-negative electrical Nyquist pulses from the AWG can be used to drive the MZM. By biasing the MZM at  $V_{\pi}$  (null), the zero-crossing points of the input electrical Nyquist pulse trains translate into the zero-power points of the output optical Nyquist pulse trains, thus meeting the Nyquist ISI-free criterion and reducing the pulse width simultaneously. The generated 10 GHz optical Nyquist pulses have been employed in sampling and demodulating 1 Gbaud 16-QAM and 32-QAM signals. At the highest carrier frequency of 22.5 GHz, the measured EVM value was lower than 6%.

The use of an expensive, general-purpose AWG for Nyquist pulse synthesis might be seen as a cost barrier to the commercialization of the technique. For specific implementations, an FPGA and a separate DAC can be employed instead.

At this stage, the current estimation of the system's ENOB is about 4.5. However, in order to measure the achievable ENOB of the photonic sampling system accurately, an optimization of the overall system is required. Indeed, future activities will focus on improving the system's performance, including MZM nonlinearity compensation and ASE noise reduction. Moreover, the employed real-time oscilloscope (ENOB of about 4.7) can be replaced with an ADC of a lower sampling rate and higher performance.

### **Funding**

United Kingdom Engineering and Physical Sciences Research Council (EPSRC) (standard grant no.: EP/M021939/1).